

Obtaining enhanced outputs from coupled stochastic heat engines

Aradhana Kumari^{1*}, Rahul Marathe^{2†} and Sourabh Lahiri^{1‡}

¹Department of Physics, Birla Institute of Technology Mesra, Jharkhand 835215, India

²Department of Physics, Indian Institute of Technology Delhi, Hauz Khas 110 016, New Delhi, India

Abstract

Recent works on coupling of two simple heat engines have shown that it may lead to non-monotonic variations in the efficiency and power with parameters like driving amplitudes and asymmetries in cycle periods. Motivated by this study, we investigate the effect of the coupling between two stochastic heat engines where colloidal particles have been trapped in harmonic potentials. The stiffness parameters of each engine are varied cyclically, but with different cycle periods, with a common thermal bath that acts as a sink for the first engine but as a source for the second. We consider two types of protocols, first where trap strength is varied linearly and the second that has sudden jumps in the trap strengths. In both we find several non-trivial effects, like the enhanced performance of the coupled engine with respect to a single effective engine, and the non-monotonic functional dependence of the engine outputs on several parameters used in the setup. A general relation of the efficiency of an arbitrary number of coupled engines driven quasistatically has been provided.

PACS: 05.40.-a, 07.20.Pe, 05.70.Ln, 05.10.Gg

1 Introduction

The challenge of theoretical and experimental study on heat engines, classical and quantum, and their potential benefits have attracted a lot of attention over the past decade or so [1–8]. The single-particle manipulation techniques have greatly boosted the experimental study of their thermodynamic properties [9, 10]. The important difference from macroscopic thermal engines is the presence of appreciable thermal noise at microscopic scales, thus implying that microscopic thermal machines are not just the naive scaled-down version of their macroscopic counterparts [11].

The working system in most of the theoretical investigations on classical heat engines and refrigerators includes a colloidal particle following an overdamped Langevin equation. Several generalizations have been made thereafter, including the case of replacing the simple Brownian particles with self-propelled particles of various types, like the active Brownian particles (ABPs) [12–16], active Ornstein-Uhlenbeck particles (AOUPs) [17], and run-and-tumble particles (RTPs) [16, 18]. Several extensions have been made in the quantum regime, where phenomena like squeezing [19–21], entanglement [22–24] and coherence [25–28] have been studied.

The optimization of such thermal machines has also received a major attention [29–31], since it helps in reducing the dissipation during nonequilibrium protocols, leading to increased practical applications of such machines. The optimal protocols (externally controlled time-variation of a single or more parameters) for a harmonic potential [1] and for log-harmonic

*Email: aradhanakumari2546@gmail.com

†Email: maratherahul@physics.iitd.ac.in

‡Email: sourabhlahiri@bitmesra.ac.in

potential [30] have been derived. The efficiency at maximum power has been studied in several works [1, 32–34].

In some recent works [35], the authors focus on the dependence of efficiency and power on the driving forces acting on engines that are sequentially connected to different thermal reservoirs, for both constant and linear drives. In an extension to this work [36], the authors introduce an asymmetry between the contact times with the different heat baths and the magnitude of the driving forces as possible parameters that can be used to optimize the performance.

In the present work, we build on this idea and construct a coupled engine that is placed in a harmonic trapping potential whose stiffness parameter is made time-dependent. This is in alignment with the frequently used prototypes for stochastic heat engines used in the literature [1, 2, 37–39]. We find that as long as the engine remains in the underdamped regime, in several cases we obtain interesting features in the engine outputs, as a function of various parameters that can directly affect the performance of such engines. Unfortunately, these features disappear in the overdamped limit, thus leaving the study difficult to investigate analytically, except in a special case referred to as a *jump protocol* in the text (see Sec. 2.2).

The paper is organized as follows. In Sec. 2, we discuss the model that we are investigating by means of analytics and simulations. This includes the equations of motion governing the dynamics of the working system, and the types of protocols used. In Sec. 3, we discuss the results of two coupled engine subjected to the jump protocol as well as to the linear protocol. In the former case, we compare the outcomes of simulations with analytics, and the latter protocol is studied entirely using simulations. In Sec. 4, we briefly discuss the coupling of three engines. Sec. 5 discusses the generalizations to the case where higher number of engines are coupled. Finally, we conclude in Sec. 6.

2 Model

2.1 Equations of motion

The schematic diagram of the coupled engines has been provided in figure 1. The first engine operates between two thermal baths at temperature T_1 (hot bath) and T_2 (cold bath). The cycle time for the first engine continues from $t = 0$ to $t = \tau_1$. The expansion and compression processes are each equal to $t = \tau_1/2$. Similarly, the cycle time for the second engine is of duration τ_2 and runs from $t = \tau_1$ to $t = \tau_1 + \tau_2$. Again, the cycle time of τ_2 is equally divided among the expansion step and the compression step. The time-dependence of the stiffness parameter for expansion and compression steps will be denoted by the functions $k_{e,i}(t)$ and $k_{c,i}(t)$, where $i = 1, 2$ denotes parameters for the first and second engines respectively. The first engine works between thermal baths at temperatures T_1 and T_2 respectively. This engine is coupled with the second engine such that the cold bath of the first engine plays the role of the hot bath for the second engine. Thus, the second engine operates between thermal baths at temperature T_2 (hot bath) and T_3 (cold bath).

We denote the position and velocity of the particle in the first engine by x_1 and v_1 respectively, while that for the second engine by x_2 and v_2 respectively. The equations of motion are for the first engine are

$$\begin{aligned} \frac{dx_1}{dt} &= v_1; & \frac{dv_1}{dt} &= \frac{1}{m}[-\gamma v_1 - k_{e,1}(t)x_1 + \xi_1(t)], & t &\in (0, \tau_1/2); \\ \frac{dx_1}{dt} &= v_1; & \frac{dv_1}{dt} &= \frac{1}{m}[-\gamma v_1 - k_{c,1}(t)x_1 + \xi_2(t)], & t &\in (\tau_1/2, \tau_1). \end{aligned} \quad (1)$$

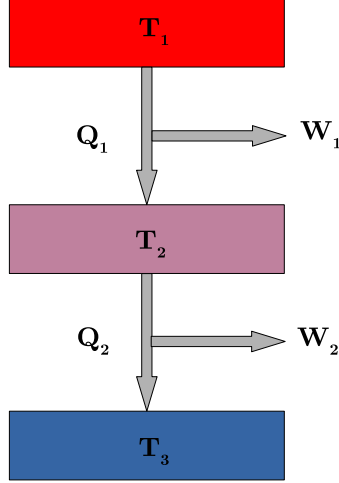


Figure 1: Schematic diagram showing two coupled stochastic heat engines

and for the second engine are

$$\begin{aligned} \frac{dx_2}{dt} &= v_2; & \frac{dv_2}{dt} &= \frac{1}{m}[-\gamma v_2 - k_{e,2}(t)x_2 + \xi_2(t)], & t &\in (\tau_1, \tau_1 + \tau_2/2); \\ \frac{dx_2}{dt} &= v_2; & \frac{dv_2}{dt} &= \frac{1}{m}[-\gamma v_2 - k_{c,2}(t)x_2 + \xi_3(t)], & t &\in (\tau_1 + \tau_2/2, \tau_1 + \tau_2). \end{aligned} \quad (2)$$

The Gaussian white noise terms follow the relations $\langle \xi_i(t) \rangle = 0$ and $\langle \xi_i(t) \xi_j(t') \rangle = 2\gamma T_i \delta_{ij} \delta(t-t')$, where $i, j = 1, 2, 3$. For convenience, the Boltzmann constant has been set to unity throughout this article.

2.2 Protocols used

We consider two simple functional forms of the time dependent stiffness parameter. These are the popular functional forms among the ones used in the literature [13, 17, 18].

1. **Sudden jump:** The stiffness parameter undergoes a sudden jump mid-way during the expansion and compression processes. For engine 1, this can be mathematically stated as:

$$\begin{aligned} k_{e,1} &= k_0, & t &\leq \tau_1/4; \\ k_{e,1} &= k_0/2, & \tau_1/4 < t &\leq \tau_1/2; \\ k_{c,1} &= k_0/2, & \tau_1/2 < t &\leq 3\tau_1/4; \\ k_{c,1} &= k_0, & 3\tau_1/4 < t &\leq \tau_1. \end{aligned} \quad (3)$$

Similar equations can be set up for the second engine, where the jumps take place at time instances $t = \tau_1 + \tau_2/4$ (expansion) and $t = \tau_1 + 3\tau_2/4$ (compression), respectively. The form of stiffness parameter for the complete cycle is shown in figure 2. This model is analytically solvable and hence can be used to verify the agreement with our simulations.

2. **Linear variation:** In this case, the stiffness parameter decreases linearly with time during the expansion half for each engine, and increases during the other half. For the first engine,

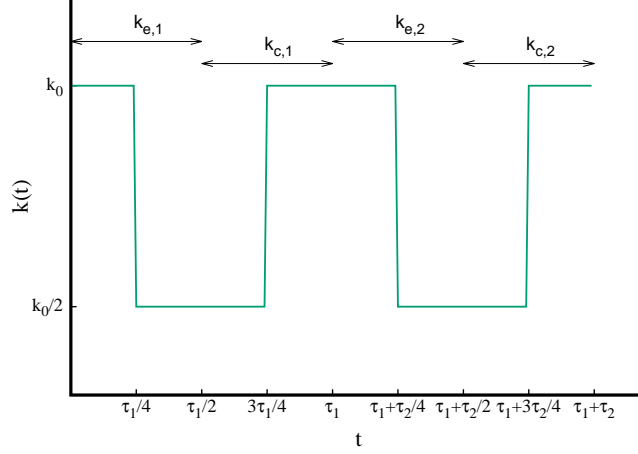


Figure 2: Variation in the stiffness parameter with time for sudden jump process.

the relations become

$$\begin{aligned}
 k_{e,1}(t) &= k_0(1 - t/\tau_1), & t &\leq \tau_1/2; \\
 k_{c,1}(t) &= k_0(t/\tau_1), & \tau_1/2 < t &\leq \tau_1; \\
 k_{e,2}(t) &= k_0[1 - (t - \tau_1)/\tau_2], & \tau_1 < t &\leq \tau_1 + \tau_2/2; \\
 k_{c,2}(t) &= k_0[(t - \tau_1)/\tau_2], & \tau_1 + \tau_2/2 < t &\leq \tau_1 + \tau_2.
 \end{aligned} \tag{4}$$

Here, $k_{e,i}$ and $k_{c,i}$ (with $i = 1, 2$) are the stiffness parameters of the i^{th} engine during the expansion and compression strokes, respectively. The time-variation of this protocol is shown in figure 3. The system is not analytically solvable in this case, and we need to investigate it by means of simulations.

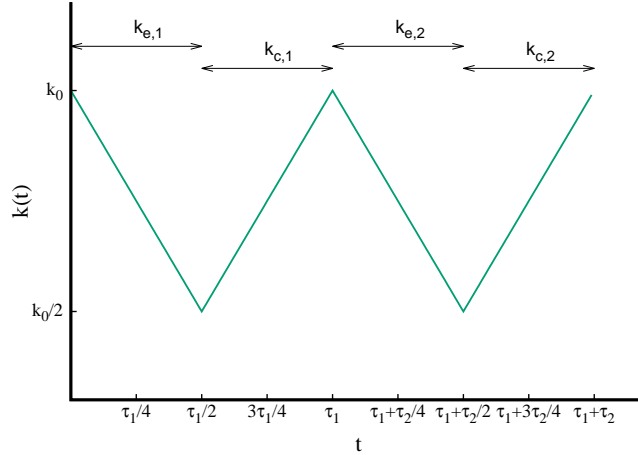


Figure 3: Variation in linearly dependent stiffness parameter with time.

2.3 Work and Heat

The average input and output work are defined as per the prescription of stochastic energetics provided in [40, 41]. It is to be noted that for our system of coupled engines, the *input* work is equal to the output work obtained from the first engine, since this work is fed into the input of the second engine [35]. The output work, on the other hand, is the one that is extracted

from the second engine, since that is the overall output of the coupled system. We define $\sigma_e(t)$ and $\sigma_c(t)$ to be the variances $\langle x^2(t) \rangle$ (angular brackets denote ensemble averages) during the expansion and compression steps, respectively. The mean input and output works are as follows:

$$\begin{aligned}\langle W_1 \rangle &= \frac{1}{2} \int_0^{\tau_1/2} \dot{k}_{e,1}(t) \sigma_e(t) dt + \frac{1}{2} \int_{\tau_1/2}^{\tau_1} \dot{k}_{c,1}(t) \sigma_c(t) dt \\ \langle W_2 \rangle &= \frac{1}{2} \int_{\tau_1}^{\tau_1+\tau_2/2} \dot{k}_{e,2}(t) \sigma_e(t) dt + \frac{1}{2} \int_{\tau_1+\tau_2/2}^{\tau_1+\tau_2} \dot{k}_{c,2}(t) \sigma_c(t) dt.\end{aligned}\quad (5)$$

The dissipated heats (note that the absorbed heat is obtained by simply switching the sign) of the first and second engines, denoted by Q_1 and Q_2 , are readily obtained by applying the first law:

$$\begin{aligned}\langle Q_1 \rangle &= \langle W_1 \rangle - \langle \Delta E_1 \rangle \\ \langle Q_2 \rangle &= \langle W_2 \rangle - \langle \Delta E_2 \rangle,\end{aligned}\quad (6)$$

where the change in internal energy is defined as the difference between the total (potential plus kinetic) energies at the beginning and at the end of the expansion step:

$$\begin{aligned}\langle \Delta E_1 \rangle &= \left[\frac{1}{2} k(\tau_1/2) \sigma(\tau_1/2) + \frac{1}{2} m \sigma_v(\tau_1/2) \right] - \left[\frac{1}{2} k(0) \sigma(0) + \frac{1}{2} m \sigma_v(0) \right] \\ \langle \Delta E_2 \rangle &= \left[\frac{1}{2} k(\tau_1 + \tau_2) \sigma(\tau_1 + \tau_2) + \frac{1}{2} m \sigma_v(\tau_1 + \tau_2) \right] \\ &\quad - \left[\frac{1}{2} k(\tau_1 + \tau_2/2) \sigma(\tau_1 + \tau_2/2) + \frac{1}{2} m \sigma_v(\tau_1 + \tau_2/2) \right]\end{aligned}\quad (7)$$

The efficiency of coupled heat engine is defined as:

$$\eta = \frac{\langle W_2 \rangle}{\langle W_1 \rangle + \langle Q_1 \rangle + \langle Q_2 \rangle} = \frac{W_{\text{out}}}{W_{\text{in}} + Q_{\text{in}} + Q_{\text{out}}}, \quad (8)$$

where we have defined $W_{\text{in}} \equiv -\langle W_1 \rangle$, $W_{\text{out}} \equiv -\langle W_2 \rangle$, $Q_{\text{in}} \equiv -\langle Q_1 \rangle$, and $Q_{\text{out}} \equiv -\langle Q_2 \rangle$. The minus sign appears due to our convention to consider the heat dissipated by the system and the work done on the system as positive.

3 Results and Discussions

3.1 Case 1: Sudden jump protocol

We first choose case 1 outlined in Sec. 2, where the expansion and compression halves involve sudden jumps in the stiffness parameters at the mid-point of the respective halves. The Langevin equations can be conveniently written as the following matrix equation:

$$\frac{d\mathbf{A}}{dt} = -\mathbf{M} \cdot \mathbf{A} + \mathbf{\Xi}(t), \quad (9)$$

For instance, for the expansion step of the first engine, the matrices are

$$\mathbf{A} = \begin{pmatrix} x \\ v \end{pmatrix}; \quad \mathbf{M} = \begin{pmatrix} 0 & -1 \\ k_{e,1}/m & \gamma/m \end{pmatrix}; \quad \mathbf{\Xi}(t) = \begin{pmatrix} 0 \\ \xi_1(t)/m \end{pmatrix}. \quad (10)$$

Here, the values of $k_{e,1}$ are given by Eq. (3). The formal solution to the above equation is given by

$$\mathbf{A}(t) = \mathbf{A}(0)e^{-\mathbf{M}t} + \int_0^t e^{-\mathbf{M}(t-t')} \mathbf{\Xi}(t') dt'. \quad (11)$$

If the initial conditions for the first cycle are given by $x(0) = 0$ and $v(0) = 0$, then the variances for the expansion half of this cycle can be found from the relation

$$\begin{aligned} \langle A(t)A^T(t) \rangle &= \begin{pmatrix} \langle x_1^2 \rangle & \langle x_1 v_1 \rangle \\ \langle x_1 v_1 \rangle & \langle v_1^2 \rangle \end{pmatrix} \equiv \begin{pmatrix} \sigma_{x_1} & \sigma_{x_1 v_1} \\ \sigma_{x_1 v_1} & \sigma_{v_1} \end{pmatrix} \\ &= \int_0^t dt' \int_0^t dt'' e^{-\mathbf{M}(t-t')} \langle \mathbf{\Xi}(t') \mathbf{\Xi}^T(t'') \rangle e^{-\mathbf{M}^T(t-t'')}. \end{aligned} \quad (12)$$

Similar solutions can be obtained for the compression half as well, and can be extended to the second engine. It is to be noted that the initial conditions for the compression half must be equal to the final values of x and v reached at the end of the expansion half, i.e. $A(\frac{\tau}{2}^+) = A(\frac{\tau}{2}^-)$.

The analytical expressions for the variances in position and velocity for the expansion stroke of the first engine during the first cycle are as given below.

$$\begin{aligned} \sigma_x(t) &= \frac{T_1}{2k_0\alpha^2} e^{-(\gamma+\alpha)t/m} \left[\gamma(\gamma+\alpha)e^{2\alpha t/m} + \gamma(\gamma-\alpha) - 8k_0 m e^{\alpha t/m} - 2\alpha^2 e^{(\gamma+\alpha)t/m} \right]; \\ \sigma_v(t) &= \frac{T_1}{m\alpha^2} e^{-(\gamma+\alpha)t/m} \left[8k_0 m e^{\alpha t/m} + 2\alpha^2 e^{(\gamma+\alpha)t/m} + \gamma(\alpha-\gamma)e^{2\alpha t/m} - \gamma(\gamma+\alpha) \right]. \end{aligned} \quad (13)$$

Similar expressions for the variances during the other strokes can be obtained, using the final values of the previous stroke as the initial values for the next stroke.

Repeating the process for the second engine as well, we can obtain the variances and work in the full cycle ($\tau_1 + \tau_2$) of the coupled engine. Using these expressions we can also find analytical expressions for work and heat. However, they are too long to be included here. Fig. 4(a) and (b) show the agreement of the results of numerical integration with the simulated ones, for the variances in position and velocity respectively, obtained from Eq. (1) for the first cycle of the coupled engine with the jump protocol given in Eq. (3). The Heun's method of integration has been used in our simulations, and the ensemble averaging has been carried out over 10^5 experimental realizations.

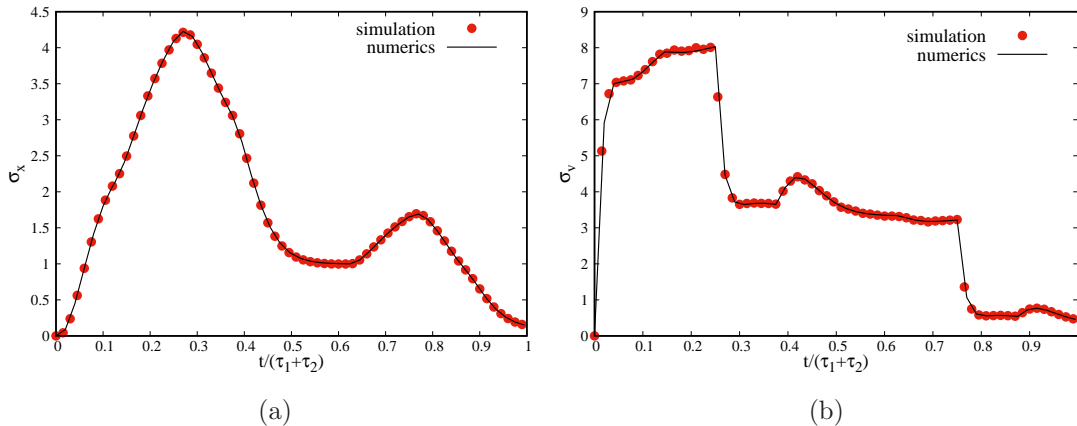


Figure 4: (a) Plot of the position variance obtained from numerical integration for a full cycle of the coupled engine, and its comparison with simulation. Both x and v begin from zero at $t = 0$. (b) Similar plot for variance in velocity. The parameters used in the above figures are: $m = 0.3$, $T_1 = 2.5$, $T_2 = 1$, $T_3 = 0.1$, $k_0 = 1$, $\gamma = 1$, $\tau_1 = 5$, $\tau_2 = 5$.

Fig. 5 shows the comparison between simulation and analytics for the work done on the engine, as a function of the time asymmetry $t_{\text{asy}} = \tau_1/\tau_2$. The clear agreement between the analytical results with the simulated ones are clearly observed. Figs. 4 and 5 thus complete the bench marking of our simulated outcomes. Henceforth, the latter would be extended to the steady state regime, where the initial transients would be removed in order to study the behaviour of the engine when its distribution functions have become time-periodic.

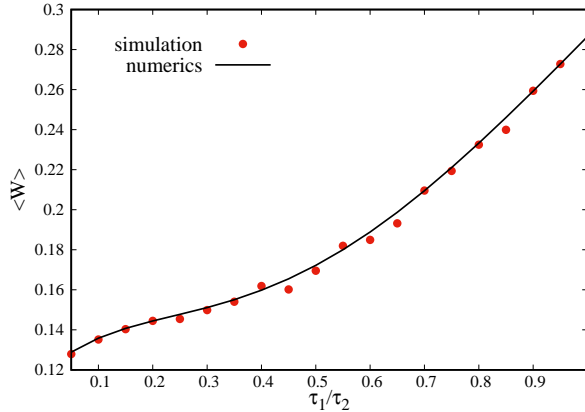


Figure 5: Plot of analytically obtained total work, i.e., $\langle W \rangle = \langle W_1 \rangle + \langle W_2 \rangle$, with t_{asy} , and its comparison with simulation. The other parameters used in the above figures are the same as in Fig. 4.

The plots for efficiency and power of the coupled engine operated by the jump protocol, as a function of the time asymmetry $t_{\text{asy}} = \tau_1/\tau_2$, has been shown in Fig. 6, for the set of parameters mentioned in the figure caption. We find a clear non-monotonicity in efficiency, with the maximum occurring at a small value of $t_{\text{asy}} \ll 1$. For comparison, the behaviour of a single engine operating directly between the first and the third heat baths (at temperatures T_1 and T_3 , respectively) has been shown (magenta line with solid circles). The single engine runs for a cycle time equal to that of the full cycle time of the coupled engine, i.e.

$$\tau_{\text{single}} = \tau_1 + \tau_2. \quad (14)$$

This means that the expansion/compression steps of engine 1 (of duration $\tau_1/2$ each) and the expansion/compression steps of engine 2 (of duration $\tau_2/2$ each) are of half the duration as the expansion/compression steps of the single engine. Note that this is the most reasonable comparison that can be made between the coupled and single engines in our setup.

Fig. 6(b) shows the output power as a function of t_{asy} . Although the non-monotonicity in the case of coupled engines is not prominent, it can be clearly observed for the single engine. We have checked separately that the main contributors to the non-monotonicity of efficiency (out of the four thermodynamic variables appearing in the definition of efficiency, see Eq. (8)), are the input work $W_{\text{in}} = -\langle W_1 \rangle$ and the output heat $Q_{\text{out}} = -\langle Q_2 \rangle$, both of which are observed to show a maximum at $\tau_1/\tau_2 \approx 0.4$.

3.2 Case 2: Linearly varying stiffness parameters

In Fig. 7(a) and (b), we have shown the simulated variances in position and velocity as a function of time in the full engine cycle of duration $\tau_1 + \tau_2$. A comparison with Fig. 4 shows that the qualitative trends are similar, while are relatively close quantitatively. Again, the two peaks in position variance correspond to the switching from expansion to compression step in the case of each of the coupled engines.

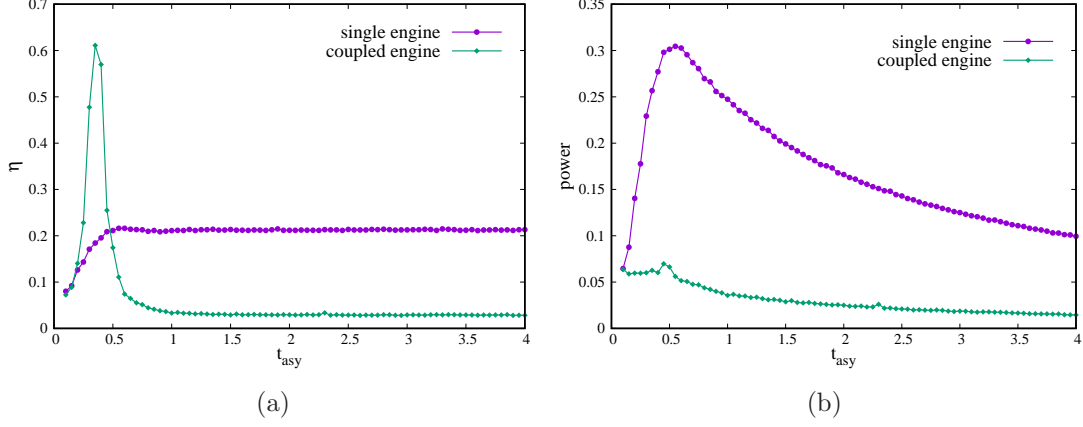


Figure 6: (a) Plot of efficiency as a function of t_{asy} for sudden jump process; (b) Similar plot of power with t_{asy} . The parameters used are: $k_0 = 10$, $m = 0.1$, $T_1 = 2$, $T_2 = 1$, $T_3 = 0.1$, $\tau_2 = 1$, $\gamma = 1$.

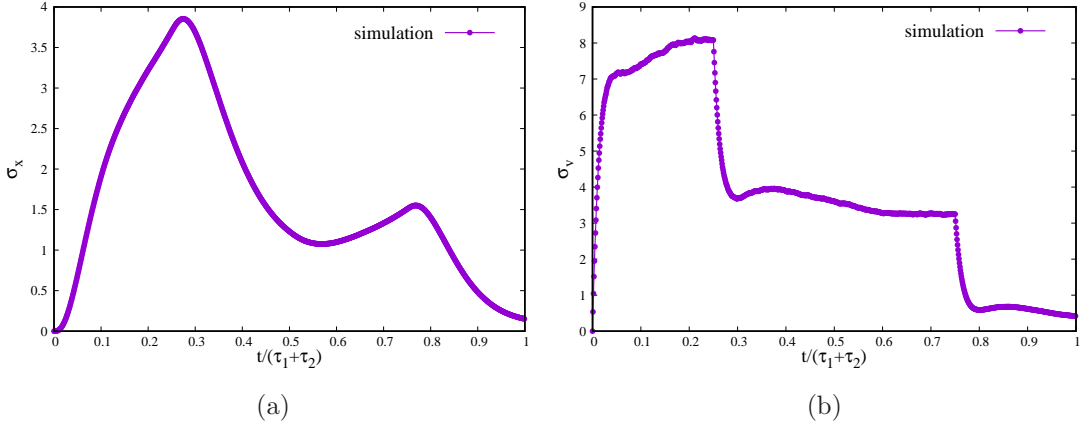


Figure 7: (a) Plot of variance in position for a full cycle of coupled engine for the case of linearly dependent stiffness parameter, when both x and v begin from zero at $t = 0$. (b) Similar plot for variance in velocity. The parameters are: $m = 0.3$, $T_1 = 2.5$, $T_2 = 1$, $T_3 = 0.1$, $k_0 = 1$, $\gamma = 1$, $\tau_1 = 5$, $\tau_2 = 5$.

The efficiency of a coupled heat engine with the time asymmetry t_{asy} is plotted in Fig. 8(a). The red solid line with solid triangles is the reference curve that shows the variation of η with t_{asy} for a single engine working between T_1 and T_3 (see Fig. 1). The plot shows that for $t_{\text{asy}} = 1$ (i.e time period of the first engine is equal to the time period of the second engine), the efficiency of coupled engine is less than from that of the single engine with same parameters, as expected in equilibrium thermodynamics (see Sec. 5). In the region where $t_{\text{asy}} \leq 0.5$, the plot shows non-monotonic variation of efficiency with t_{asy} , where it outperforms the single engine. A peak is observed for all the three values of k_0 but at different values of t_{asy} , all being present in the region $\tau_1 < \tau_2$. The fact that the efficiency becomes higher for smaller values of t_{asy} can be argued as follows: since the cycle time of the first engine τ_1 is smaller than that of the second engine τ_2 , it reduces W_{in} as well as Q_{in} , both of which appear in the denominator of the expression in the right hand side of (8). At the same time, W_{out} also increases in this region, as can be seen from Fig. 8(b). We clearly see that the region $t_{\text{asy}} < 1$ shows peak in the power for all values of k_0 used in our simulations. Thus, the interplay of these quantities lead to a peak in the efficiency when $\tau_1 < \tau_2$. We further note from Fig. 8(b) that higher values of k_0 lead to extraction of higher power from the coupled engine. However, except near the peaks, the single engine (red solid line with triangles) outperforms the coupled ones almost for all values

of t_{asy} , in terms of output power. Thus, to enjoy the perks of the coupling, one must explore the regime where $t_{\text{asy}} < 1$. The region where $t_{\text{asy}} > 1$ does not show any interesting feature, as expected from the fact that the W_{out} decreases and W_{in} increases when $\tau_1 > \tau_2$, so that the efficiency show a monotonic decay (see Eq. (8)).

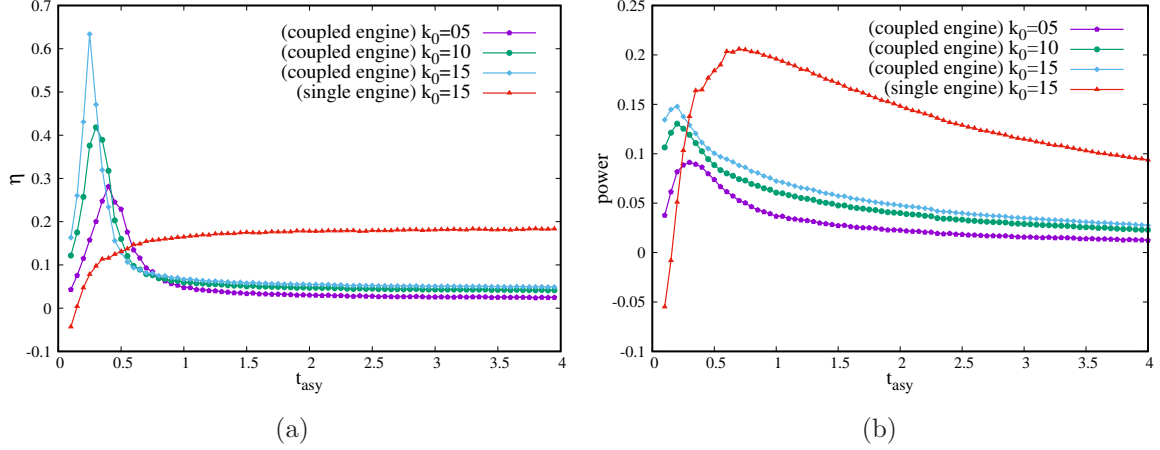


Figure 8: (a) The Plots show efficiency for the coupled engine with linearly varying protocol, with asymmetric time for $k_0 = 5$ (purple line), $k_0 = 10$ (green line), $k_0 = 15$ (cyan line). (b) Similar plot for the magnitude of extracted power. The other used parameters are: $T_1 = 2$, $T_2 = 1$, $T_3 = 0.1$, $m = 0.1$.

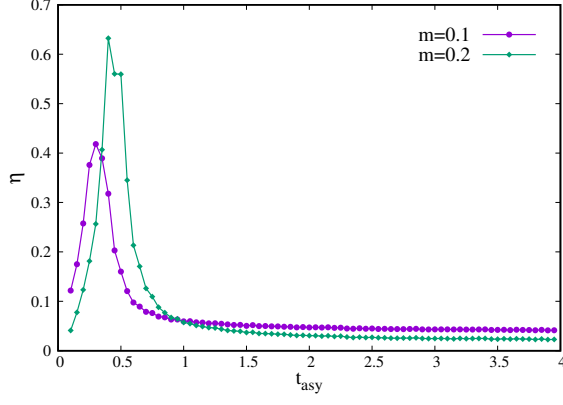
We next move to figure 9, where the variation of efficiency (figure 9(a)) and power (figure 9(b)) with mass have been shown. We find that if mass is increased, the peak value of both quantities shift towards smaller values of t_{asy} . With this region, the efficiency increases but the extracted power decreases with increase in mass, once again highlighting the interplay of the different thermodynamic observables appearing in the definition of efficiency, vide Eq. 8.

In Fig. 10(a), we have plotted the efficiency of the coupled engine as a function of the cycle time τ_2 of the second engine, keeping the ratio $t_{\text{asy}} = \tau_1/\tau_2$ fixed ($t_{\text{asy}} = 0.5$ in this case). We find that the value of efficiency quickly saturates to a constant value. The saturation is slower if the particles is more massive, although the final saturated value is the same in the two cases: $\eta \approx 0.1$. In Fig. 10(b), similar plots have been made for the power extracted from the engine. It is clear from the figure that the power depends on the absolute values of the cycle times τ_1 and τ_2 , even if their ratios are kept constant. The plots for two different masses merge at high values of τ_2 , as shown in the figure, which indicates an identical behaviour (independent of mass) of the engine in the limit of slow driving.

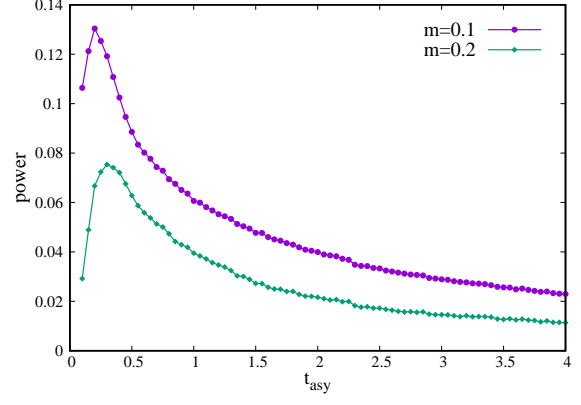
We study in Fig. 11(a) the dependence of efficiency on the stiffness parameter k_0 and the cycle time asymmetry t_{asy} . The non-monotonicity in efficiency as a function of $t_{\text{asy}} \leq 0.5$, visible as a tongue-shaped patch, in agreement with Fig. 8(a). This non-monotonicity is also present in the functional dependence of power on t_{asy} as shown in Fig. 11(b), which is again consistent with the observations on Fig. 8(b). The increase of output power with the stiffness parameter is also evident.

Fig. 12 shows the dependence of the product of efficiency and power, known as *efficient power* (EP), as a function of t_{asy} . It is a useful quantifier for the efficacy of an engine [42, 43]. This is because when the EP is maximized, the engine has both efficiency and power at a reasonably high value. The plots show that the coupled engine shows a peak in EP as well, in a narrow range of t_{asy} .

The efficiency at maximum power, denoted by η^* , can be obtained in our parameter space using Figs. 8(a) and (b). The variation of EP and η^* with the ratio of temperatures T_1/T_3 have been plotted in Fig. 13(a) and (b), respectively. Both the figures show that the coupled

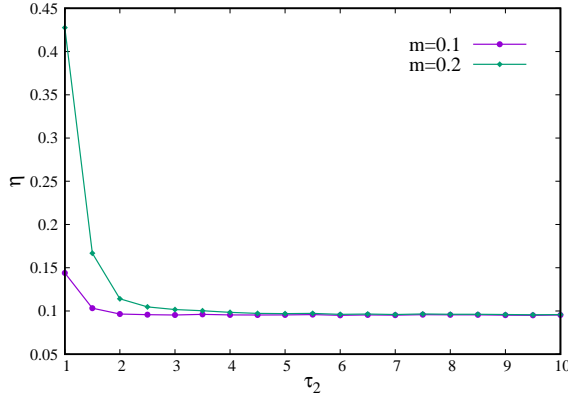


(a)

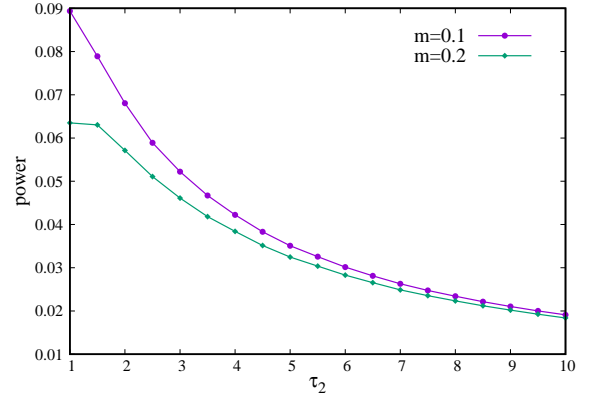


(b)

Figure 9: (a) Plots showing efficiency as a function of t_{asy} for $m = 0.1$ (purple line) and $m = 0.2$ (green line). (b) Plots showing power as a function of t_{asy} . The parameters are: $T_1 = 2$, $T_2 = 1$, $T_3 = 0.1$, $k_0 = 10$, $\tau_2 = 1$.

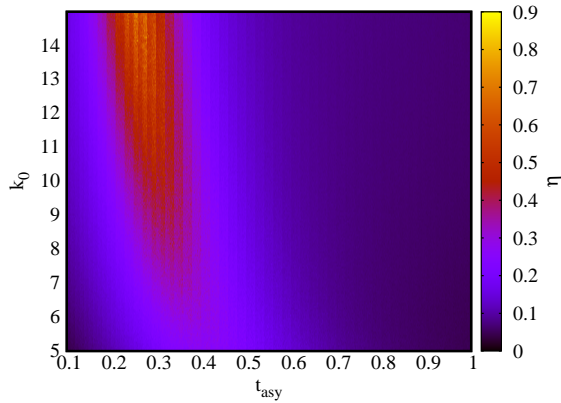


(a)

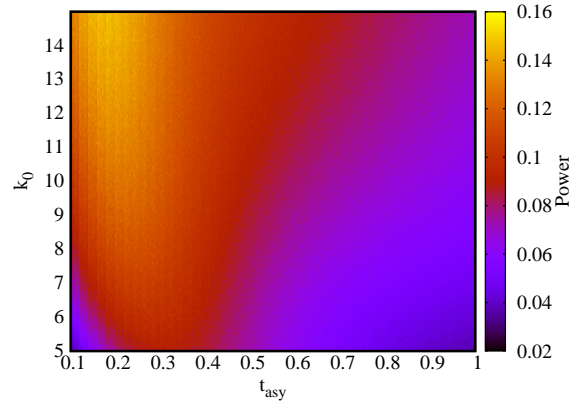


(b)

Figure 10: (a) Plots showing efficiency as a function of τ_2 , for a fixed value of t_{asy} , for $m = 0.1$ (purple line) and $m = 0.2$ (green line). (b) Plots showing power as a function of τ_2 . The parameters are: $t_{asy} = 0.5$, $T_1 = 2$, $T_2 = 1$, $T_3 = 0.1$, $k_0 = 10$.



(a)



(b)

Figure 11: Phase plot of (a) efficiency and (b) magnitude of extracted power, as a function of k_0 and t_{asy} . The other parameters are: $T_1 = 2$, $T_2 = 1$, $T_3 = 0.1$, $m = 0.1$.

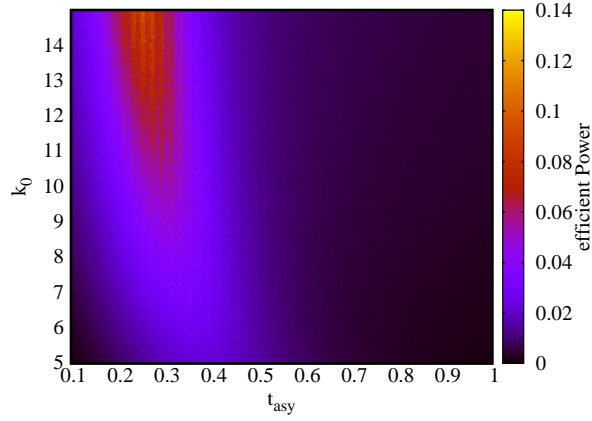


Figure 12: Phaseplot of efficient power (product of efficiency and magnitude of extracted power) as a function of k_0 and t_{asy} . The other parameters are: $T_1 = 2$, $T_2 = 1$, $T_3 = 0.1$, $m = 0.1$.

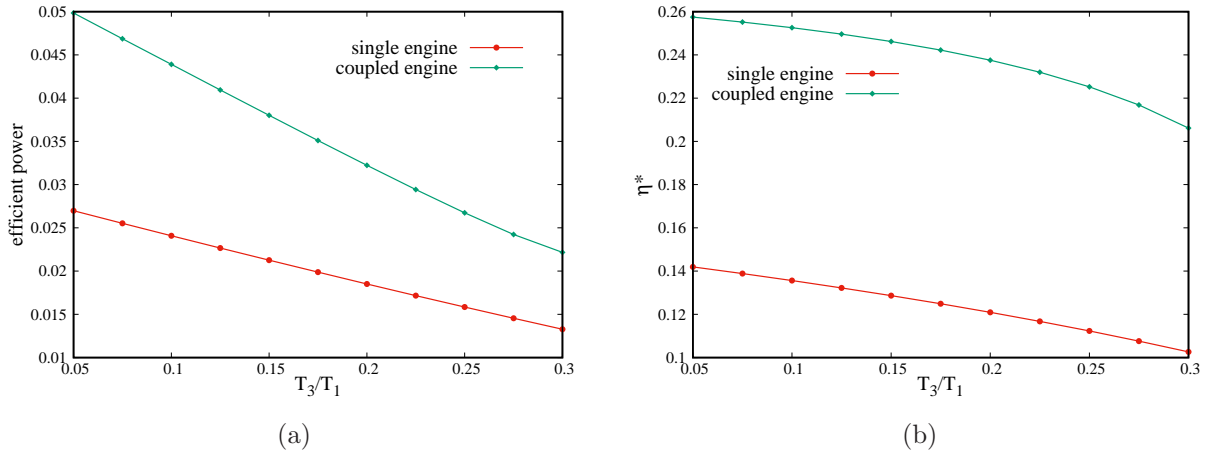


Figure 13: (a) The plot shows the variation of the efficient power with T_3/T_1 . (b) Similar plot for the efficiency at maximum power. The other parameters are: $k_0 = 10$, $m = 0.1$, $\gamma = 1$, $T_1 = 2$

engine performs better than a single engine working between the temperatures T_1 and T_3 in our parameter space.

Overall, the coupling between two different nonequilibrium heat engines seems to exhibit enhanced performance in a suitable range of parameters. It should thus be beneficial to identify the parameter range that is conducive to its performance. The role of the cycle time asymmetry is evident as well. The non-monotonicity of the engine outputs, as well as the enhanced performance with respect to single engine counterparts, both are observed at relatively smaller values of t_{asy} , where the first engine is driven much faster than the second one. The effect of nonequilibrium dynamics is demonstrated in Fig. 10, where the efficiencies seem to settle into a constant value when the driving is slow enough (τ_1 , τ_2 large), i.e. when the process begins to get closer to a quasistatic one. As the figure shows, for a highly nonequilibrium process, the efficiency shows a dependence on the absolute cycle times of the individual engines that have been coupled.

4 Three coupled engines

We now extend the treatment for two coupled engines to three coupled engines. The three engines are coupled sequentially such that the first engine operates between two thermal baths at temperature T_1 (hot bath) and T_2 (cold bath), second engine between T_2 (hot bath) and T_3 (cold bath) and third engine between temperature T_3 (hot bath) and T_4 (cold bath). The schematic diagram is given in Fig. 14.

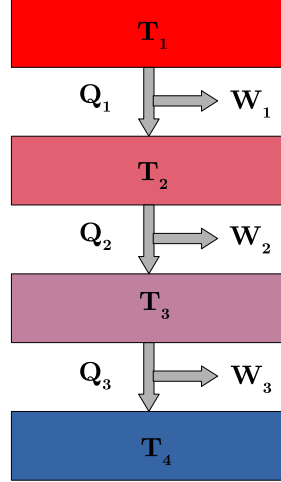


Figure 14: Schematic diagram showing three coupled stochastic heat engine.

We define the cycle time asymmetry in this case as the square of the ratio between the cycle time of engine 2 and the geometric mean of the cycle times of engines 1 and 3:

$$t_{\text{asy}} = \frac{\tau_2^2}{\tau_1 \tau_3}. \quad (15)$$

Fig. 15 (a) and (b) show the variations in the efficiency and power as a function of t_{asy} , respectively. Both these parameters show a monotonic decay with increase in the time asymmetry, as observed for several different values of the temperature ratio T_4/T_1 .

5 Analytical study of coupled engines driven quasistatically

Efficiency of Stirling Engine in quasistatic case. We now study the efficiency of multiple coupled Stirling's engines, when each is driven quasistatically. The analytical expressions for these efficiencies are derived below. The expressions would help us understand the role played by the nonequilibrium nature of our driving protocols. In fact, we find that the efficiency of coupled engine will always be less than that of a single engine in this regime. We have observed violations of this relation in the case of two coupled engines, where in a narrow range the coupled engine outperformed the single engine (see Figs. 6(a) and 8(a)).

Below, we obtain the expressions for the efficiencies of single, two and three coupled engines, and thereafter provide the general expression for n -coupled engines, n being any positive integer.

Single Stirling engine: First, we consider a single Stirling engine in the quasistatic regime where the engine works between the baths at temperature T_1 and T_2 , with $T_1 > T_2$. The *total*

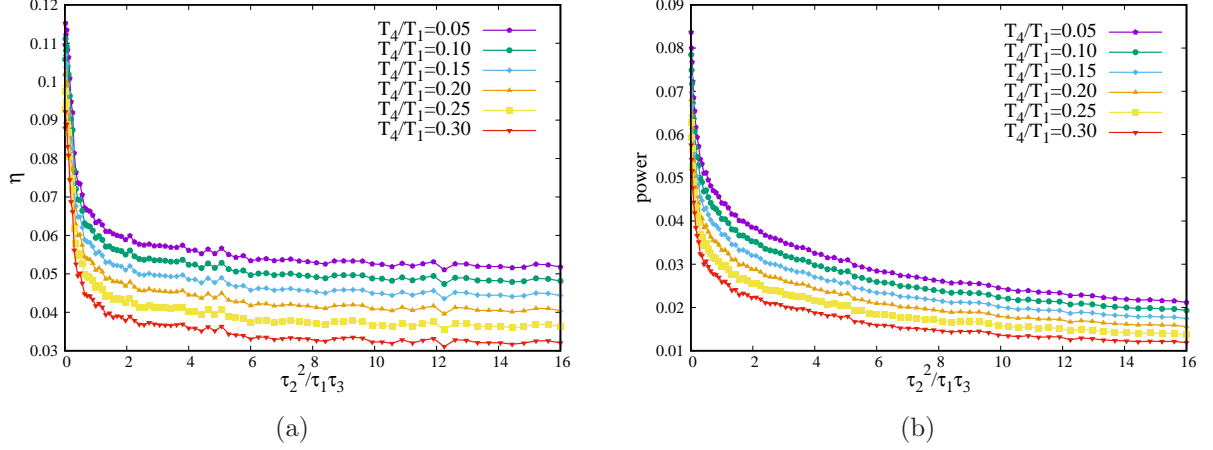


Figure 15: (a) Plots showing the variation of efficiency for three coupled engines with t_{asy} . (b) Similar plots for magnitude of extracted power with t_{asy} . The other parameters are: $T_1 = 2$, $T_2 = 1.5$, $T_3 = 1$, $\tau_1 = 1$, $\tau_3 = 1$, $\gamma = 1$, $m = 0.1$, $k_0 = 10$.

work done in the entire cycle is given by [17]

$$\langle W_1 \rangle = -\frac{T_1}{2} \ln \left[\frac{k_{\max}}{k_{\min}} \right] \left(1 - \frac{T_2}{T_1} \right), \quad (16)$$

The subscript label includes the engine number, which is trivially 1 for a single engine. while the work done on the engine during the expansion stroke is

$$\langle W_{h(1)} \rangle = -\frac{T_1}{2} \ln \left[\frac{k_{\max}}{k_{\min}} \right]. \quad (17)$$

The internal energy change during the expansion stroke is

$$\langle \Delta E_1 \rangle = \frac{T_1}{2} \left(1 - \frac{T_2}{T_1} \right). \quad (18)$$

On applying the First Law, $Q_{h(1)} = W_{h(1)} - \Delta E_1$ (true even for a single realization), one can obtain the heat absorbed (given by $-\langle Q_{h(1)} \rangle$) during expansion.

The efficiency is now readily obtained:

$$\begin{aligned} \eta_1 &= \frac{\langle W_1 \rangle}{\langle W_{h(1)} \rangle - \langle \Delta E_1 \rangle} \\ &= \frac{-\frac{T_1}{2} \ln \left[\frac{k_{\max}}{k_{\min}} \right] \left(1 - \frac{T_2}{T_1} \right)}{-\frac{T_1}{2} \ln \left[\frac{k_{\max}}{k_{\min}} \right] - \frac{T_1}{2} \left(1 - \frac{T_2}{T_1} \right)} \\ &= \frac{T_1 - T_2}{T_1 + \alpha_1} \end{aligned} \quad (19)$$

where, $\alpha_1 = (T_1 - T_2) \left[\ln \left(\frac{k_{\max}}{k_{\min}} \right) \right]^{-1}$.

Two coupled Stirling Engines: The schematic diagram has been shown in Fig. 1, with $T_1 > T_2 > T_3$. We denote by W_i , with $i = 1, 2$, as the works done during the i^{th} engine's cycle, and the corresponding dissipated heats during expansion strokes by $Q_{h(i)}$. The works absorbed

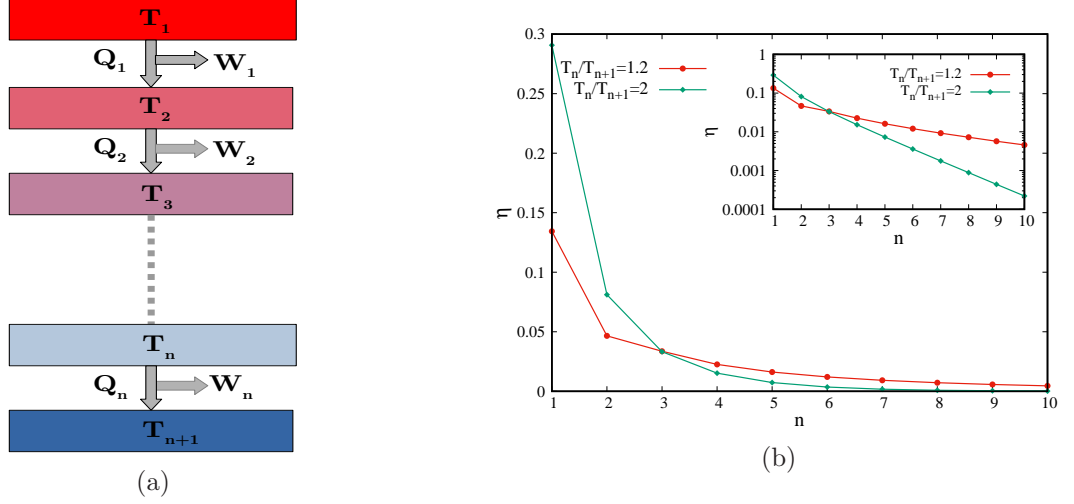


Figure 16: (a) Schematic diagram showing n coupled engines. (b) Plot showing the efficiency with number of engines n . The ratio of the stiffness parameter is kept fixed at $k_{\max}/k_{\min}=2$. Inset shows the same plots in a semi-log scale.

by engines 1 and 2 (negatives of the works extracted) are respectively

$$\begin{aligned}\langle W_1 \rangle &= -\frac{T_1}{2} \ln \left[\frac{k_{\max}}{k_{\min}} \right] \left(1 - \frac{T_2}{T_1} \right) \\ \langle W_2 \rangle &= -\frac{T_2}{2} \ln \left[\frac{k_{\max}}{k_{\min}} \right] \left(1 - \frac{T_3}{T_2} \right).\end{aligned}\quad (20)$$

$$\begin{aligned}\langle Q_{h(1)} \rangle &= \langle W_{h(1)} \rangle - \langle \Delta E_1 \rangle \\ &= -\frac{T_1}{2} \ln \left[\frac{k_{\max}}{k_{\min}} \right] - \frac{T_1}{2} \left(1 - \frac{T_2}{T_1} \right)\end{aligned}\quad (21)$$

Similarly,

$$\langle Q_{h(2)} \rangle = -\frac{T_2}{2} \ln \left[\frac{k_{\max}}{k_{\min}} \right] - \frac{T_2}{2} \left(1 - \frac{T_3}{T_2} \right).\quad (22)$$

The efficiency can now be readily calculated:

$$\begin{aligned}\eta_2 &= \frac{\langle W_2 \rangle}{\langle W_1 \rangle + \langle Q_{h(1)} \rangle + \langle Q_{h(2)} \rangle} \\ &= \frac{T_2 - T_3}{T_1 + \alpha_2},\end{aligned}\quad (23)$$

where $\alpha_2 = T_1 + (T_1 - T_3) [\ln(k_{\max}/k_{\min})]^{-1}$. Clearly, cycle time asymmetry does not contribute to the efficiency in this limit.

Three coupled Stirling Engines: The three engines are coupled in a way shown in Fig. 14, such that $T_1 > T_2 > T_3 > T_4$. Proceeding as before, we obtain

$$\begin{aligned}\eta_3 &= \frac{\langle W_3 \rangle}{\langle W_1 \rangle + \langle W_2 \rangle + \langle Q_{h(1)} \rangle + \langle Q_{h(2)} \rangle + \langle Q_{h(3)} \rangle} \\ &= \frac{T_3 - T_4}{2T_1 + T_2 + (T_1 - T_4) [\ln(k_{\max}/k_{\min})]^{-1}} \\ &= \frac{T_3 - T_4}{T_1 + \alpha_3},\end{aligned}\quad (24)$$

where $\alpha_3 = (T_1 + T_2) + (T_1 - T_4) [\ln(k_{\max}/k_{\min})]^{-1}$.

General case: n coupled stirling Engines: It is easy to extend the treatment to n coupled engines. The couplings are as shown in Fig. 16(a), with $T_1 > T_2 > T_3 > T_4 > \dots > T_n > T_{n+1}$. The efficiency is given by

$$\begin{aligned}\eta_n &= \frac{\langle W_n \rangle}{\langle W_1 \rangle + \langle W_2 \rangle + \dots + \langle W_{n-1} \rangle + \langle Q_{h(1)} \rangle + \langle Q_{h(2)} \rangle + \dots + \langle Q_{h(n)} \rangle} \\ &= \frac{T_n - T_{n+1}}{T_1 + \alpha_n},\end{aligned}\tag{25}$$

where $\alpha_n = (T_1 + T_2 + \dots + T_{n-1}) + (T_1 - T_{n+1})[\ln(k_{\max}/k_{\min})]^{-1}$.

The dependence on the efficiency of coupled engines on the number (n) of engines coupled is shown in Fig. 16(b). Clearly, the efficiencies become smaller when n becomes larger, demonstrating that coupling of engines is not very useful for quasistatic driving. The inset shows the exponential decay of η_n with n . Moreover, the expression (25) shows that in the limit $n \rightarrow \infty$, the numerator becomes negligibly small when compared to the denominator, so that the efficiency goes to zero:

$$\lim_{n \rightarrow \infty} \eta_n = 0.\tag{26}$$

6 Conclusions

Coupled stochastic engines have been shown to exhibit non-trivial behaviours of efficiency and power with respect to parameters like the asymmetry in the cycle times of the engines, or the magnitude of driving. We investigate the thermodynamics of such coupled engines in the well-known setup where each engine consists of a colloidal particle confined in a harmonic trap with time-dependent stiffness. We first take up the simple case where the stiffness is made to undergo a sudden jump in the middle of both the expansion and compression steps of each engine, where analytical solutions have been provided. The results of simulations have been compared with those obtained from numerical integration, which show a very good agreement.

The calculations become intractable when the stiffness varies linearly with time, so we have studied this case by means of simulations. In both kinds of protocols, the efficiency shows a peak when the cycle time asymmetry is small. In this region, the coupled engine outperforms an equivalent single engine working between the first and the third heat baths. However, in the remaining range of t_{asy} , the single engine is more efficient. The output power of the coupled engine is almost always smaller than the single engine, except for very small values of t_{asy} . Phase plots of efficiency and power have been plotted, each as functions of k_0 and t_{asy} . They show the ranges of the latter parameters where efficiency and power exhibit non-monotonicity. The efficient power of the coupled engine is found to be larger than that of the single engine, for the chosen set of parameters.

We have also studied the variations in efficiency and power with t_{asy} three coupled engines, but they do not show non-monotonicity. Expressions of efficiency of quasistatically driven one, two and three coupled engines have been derived. Finally, a general expression for the efficiency of n coupled engines has been provided. This is followed by a discussion on the general trend of the net efficiency as more and more engines are coupled.

References

- [1] T. Schmeidl and U. Seifert. Efficiency at maximum power: An analytically solvable model for stochastic heat engines. *Europhys. Lett.*, 81:20003, 2008.
- [2] S. Rana, P. S. Pal, A. Saha, and A. M. Jayannavar. Single-particle stochastic heat engine. *Phys. Rev. E*, 90(4):042146, 2014.

- [3] J. Roßnagel, O. Abah, F. Schmidt-Kaler, K. Singer, and E. Lutz. Nanoscale heat engine beyond the carnot limit. *Phys. Rev. Lett.*, 112:030602, January 2014.
- [4] G. Verley, M. Esposito, T. Willaert, and C. Van den Broeck. The unlikely carnot efficiency. *Nat. Commun.*, 5(1):4721, 2014.
- [5] V. Blickle and C. Bechinger. Realization of a micrometre-sized stochastic heat engine. *Nat. Phys.*, 8:143, 2012.
- [6] Jonne V Koski, Ville F Maisi, Jukka P Pekola, and Dmitri V Averin. Experimental realization of a szilard engine with a single electron. *Proc. Natl. Acad. Sci. U.S.A.*, 111(38):13786–13789, 2014.
- [7] J. Roßnagel, S. T. Dawkins, K. N. Tolazzi, O. Abah, E. Lutz, F. Schmidt-Kaler, and K. Singer. A single-atom heat engine. *Science*, 352(6283):325–329, 2016.
- [8] D. von Lindenfels, O. Gräß, C. T. Schmiegelow, V. Kaushal, J. Schulz, Mark T. Mitchison, John Goold, F. Schmidt-Kaler, and U. G. Poschinger. Spin heat engine coupled to a harmonic-oscillator flywheel. *Phys. Rev. Lett.*, 123:080602, Aug 2019.
- [9] C. Bustamante, J. Liphardt, and F. Ritort. The Nonequilibrium Thermodynamics of Small Systems. *Physics Today*, 58(7):43, 2005.
- [10] F. Ritort. Single-molecule experiments in biological physics: methods and applications. *J. Phys.: Condens. Matter*, 18:R531, 2006.
- [11] C. Jarzynski. Equalities and inequalities: Irreversibility and the second law of thermodynamics at the nanoscale. *Annu. Rev. Condens. Matter Phys.*, 2(1):329–351, 2011.
- [12] A. Saha, R. Marathe, P. S. Pal, and A. M. Jayannavar. Stochastic heat engine powered by active dissipation. *J. Stat. Mech.: Theory Exp*, 2018(11):113203, nov 2018.
- [13] A. Saha and R. Marathe. Stochastic work extraction in a colloidal heat engine in the presence of colored noise. *J. Stat. Mech.: Theory Exp*, 2019(9):094012, sep 2019.
- [14] V. Holubec and R. Marathe. Underdamped active brownian heat engine. *Phys. Rev. E*, 102:060101, Dec 2020.
- [15] R. Majumdar, A. Saha, and R. Marathe. Exactly solvable model of a passive brownian heat engine and its comparison with active engines. *J. Stat. Mech.: Theory Exp*, 2022(7):073206, aug 2022.
- [16] C. A. Guevara-Valadez, R. Marathe, and J. R. Gomez-Solano. A brownian cyclic engine operating in a viscoelastic active suspension. *Physica A*, 609:128342, 2023.
- [17] A. Kumari, P. S. Pal, A. Saha, and S. Lahiri. Stochastic heat engine using an active particle. *Phys. Rev. E*, 101:032109, 2020.
- [18] A. Kumari and S. Lahiri. Microscopic thermal machines using run-and-tumble particles. *Pramana*, 95:205, Nov 2021.
- [19] J. Klaers, S. Faelt, A. Imamoglu, and E. Togan. Squeezed thermal reservoirs as a resource for a nanomechanical engine beyond the carnot limit. *Phys. Rev. X*, 7(3):031044, 2017.
- [20] J. Wang, J. He, and Y. Ma. Finite-time performance of a quantum heat engine with a squeezed thermal bath. *Phys. Rev. E*, 100:052126, Nov 2019.

- [21] A. Kumar, T. Bagarti, S. Lahiri, and S. Banerjee. Thermodynamics of one and two-qubit nonequilibrium heat engines running between squeezed thermal reservoirs. *arXiv:2209.06433*, 2022.
- [22] T. Zhang, W.-T. Liu, P.-X. Chen, and C.-Z. Li. Four-level entangled quantum heat engines. *Phys. Rev. A*, 75:062102, Jun 2007.
- [23] T. Zhang, W.-T. Liu, P.-X. Chen, and C.-Z. Li. Four-level entangled quantum heat engines. *Phys. Rev. A*, 75(6):062102, 2007.
- [24] N. Brunner, M. Huber, N. Linden, S. Popescu, R. Silva, , and P. Skrzypczyk. Entanglement enhances cooling in microscopic quantum refrigerators. *Phys. Rev. Lett.*, 89:032115, 2014.
- [25] Y.-H. Shi, H.-L. Shi, X.-H. Wang, M.-L. Hu, S.-Y. Liu, W.-Li Yang, and H. Fan. Quantum coherence in a quantum heat engine. *J. Phys. A*, 53(8):085301, jan 2020.
- [26] M. O. Scully. Extracting work from a single thermal bath via quantum negentropy. *Phys. Rev. Lett.*, 87:220601, November 2001.
- [27] M. O. Scully, K. R. Chapin, K. E. Dorfman, M. B. Kim, and Anatoly Svidzinsky. Quantum heat engine power can be increased by noise-induced coherence. *Proc. Natl. Acad. Sci. U.S.A.*, 108(37):15097–15100, 2011.
- [28] M. O. Scully, M. S. Zubairy, G. S. Agarwal, and H. Walther. Extracting work from a single heat bath via vanishing quantum coherence. *Science*, 299(5608):862–864, 2003.
- [29] N. Sánchez-Salas, L. López-Palacios, S. Velasco, and A. Calvo Hernández. Optimization criteria, bounds, and efficiencies of heat engines. *Phys. Rev. E*, 82:051101, Nov 2010.
- [30] V. Holubec. An exactly solvable model of a stochastic heat engine: optimization of power, power fluctuations and efficiency. *J. Stat. Mech.: Theory Exp*, 2014(5):P05022, may 2014.
- [31] G. Gronchi and A. Puglisi. Optimization of an active heat engine. *Phys. Rev. E*, 103:052134, May 2021.
- [32] C. Van den Broeck. Thermodynamic efficiency at maximum power. *Phys. Rev. Lett.*, 95:190602, Nov 2005.
- [33] M. Esposito, K. Lindenberg, and C. Van den Broeck. Universality of efficiency at maximum power. *Phys. Rev. Lett.*, 102:130602, Apr 2009.
- [34] M. Esposito, R. Kawai, K. Lindenberg, and C. Van den Broeck. Efficiency at maximum power of low-dissipation carnot engines. *Phys. Rev. Lett.*, 105:150603, Oct 2010.
- [35] A. L. L. Stable, C. E. Fernández Noa, W. G. C. Oropesa, and C. E. Fiore. Thermodynamics of collisional models for brownian particles: General properties and efficiency. *Phys. Rev. Research*, 2:043016, Oct 2020.
- [36] C. E. Fernández Noa, Angel L. L. Stable, William G. C. Oropesa, Alexandre Rosas, and C. E. Fiore. Efficient asymmetric collisional brownian particle engines. *Phys. Rev. Research*, 3:043152, Dec 2021.
- [37] I. A. Martinez, E. Roldan, L. Dinis, D. Petrov, J. M. R. Parrondo, and R. A. Rica. Brownian carnot engine. *Nat. Phys.*, 12:67, 2016.
- [38] V. Blickle and C. Bechinger. Realization of a micrometre-sized stochastic heat engine. *Nat. Phys.*, 8:143, 2012.

- [39] S. Krishnamurthy, S. Ghosh, D. Chatterji, R. Ganapathy, and A. K. Sood. A micrometre-sized heat engine operating between bacterial reservoirs. *Nat. Phys.*, 12:1134, 2016.
- [40] K. Sekimoto. Langevin Equation and Thermodynamics. *Prog. Theor. Phys. Supp.*, 130:17, 1998.
- [41] K. Sekimoto. *Stochastic Energetics*. Springer, 2010.
- [42] T. Yilmaz. A new performance criterion for heat engines: efficient power. *J. Energy Inst.*, 79(1):38–41, 2006.
- [43] V. Singh and R. S. Johal. Low-dissipation carnot-like heat engines at maximum efficient power. *Phys. Rev. E*, 98(6):062132, 2018.